Chemical phase segregation during the crystallization of Ge-rich GeSbTe alloys

Marta Agati, Maxime Vallet, Sébastien Joulié, Daniel Benoit, Alain Claverie

Chemical phase segregation during the crystallization of Ge-rich GeSbTe alloys

Marta Agati,[a] Maxime Vallet,[a] Sébastien Joulie,[a] Daniel Benoit,[b] Alain Claverie.[a,*]

a) CEMES-CNRS, 29 Rue Jeanne Marvig, 31055 Toulouse, France.

b) STMicroelectronics, 850 Rue Jean Monnet, 38920 Crolles, France.

marta.agati@gmail.com

maxime5vallet@gmail.com

sebastien.joulie@cemes.fr

daniel.benoit@st.com

alain.claverie@cemes.fr

* Address all correspondence to Alain Claverie at alain.claverie@cemes.fr

Key words: Phase Change Materials; GST alloys; transmission electron microscopy; phase separation; crystallization.

Abstract

Ge-rich Ge-Sb-Te alloys are foreseen materials for new non-volatile memories named Phase Change Memories offering an extended range of possible applications. However, the origin of their superior properties, notably their much higher transition temperature and increased thermal stability, is unknown. Using a variety of transmission electron microscopy based techniques, we have investigated the changes which affect the structure and composition of such alloys during thermal annealing. We show that, although Ge-rich Ge-Sb-Te materials can be grown as amorphous layers of homogeneous compositions, the primary effect of annealing is to activate phase separation between stable Ge and Ge-Sb-Te phases. This phase separation starts at 380°C while the material is still amorphous and leads to the nucleation of the first Ge nanocrystals. Increasing the annealing temperature to 400 and then 450°C allows the crystalline Ge phase to grow by driving the excess Ge out of the matrix and, finally, leads to the formation of large (30-50 nm) crystals with the face-centered-cubic Ge-Sb-Te structure. After annealing at 500°C for 30 minutes, the layer has fully crystallized and consists of a population of large (50-100 nm) face-centered-cubic Ge-Sb-Te crystals with a stoichiometry close to 225 buried in a matrix composed of small Ge nanocrystals. This study evidences that the superior properties of Ge-rich alloys do not result from the intrinsic properties of some Ge-rich crystalline phase but from kinetic factors. The formation of a two phase Ge/Ge-Sb-Te material involves long range diffusion of atomic species, first and foremost Ge.

1. Introduction

The microelectronic industry is currently facing new challenges linked to the miniaturization of electronic devices and to the increase of system functionality delivered in the same size package [1]. In this context, Phase-Change Memories (PCMs) have emerged among the most promising candidates to overcome the future technological nodes prospected for non-volatile memory technology [1-4]. Lately, PCM technology has demonstrated suitability to scaling as well as integration in large arrays with impressive data retention and endurance [1,4]. The working principle of PCMs relies on the phase transition between an amorphous (high resistive) state and a crystalline (low resistive) state, which can then be associated to the binary states of an electronic memory [2]. Furthermore, multilevel data storage concepts, exploiting intermediate resistance states, have been demonstrated to be feasible using PCMs [4-8]. The need to combine rapid switching speed and large resistivity difference between the two states has driven the interest towards the Ge-Sb-Te (GST) compounds [2]. Figure 1 shows the ternary phase diagram relative to GST compounds. Pseudo-binary $(GeTe)_x$-Sb_2Te_3 alloys as well as GeTe are located along the tie line, which represents the line of compounds which exhibit congruent melting [9]. Congruent melting exists as long as the solid phase AB and its melt have the same composition. Far from this tie line, phase separation should be expected as a result of the amorphous-to-crystal transition [9,10]. Actually, several papers report on other GST materials which do not seem to show phase separation although not belonging to the tie line, such as Ge_4SbTe_5 [11,12], $Ge_2Sb_1Te_4$ [13], $Ge_{1.5}Sb_2Te_4$ [13], $GeSb_6Te_{10}$ and $GeSb_8Te_{13}$ [10]. However, these materials are located very close to the tie line, as we can see in Fig. 1. On the other hand, although not far from the tie line, $Ge_2Sb_2Te_4$ is quite unstable and decomposes into the $Ge_1Sb_2Te_4$ and $Ge_2Sb_1Te_4$ phases [13-15]. Among the GST materials located along the tie line, $Ge_2Sb_2Te_5$ is the compound offering the best compromise between crystallization speed [16] and high

amorphous stability (i.e., high crystallization temperature) [17]. For this reason, countless studies have focused on the investigation of $Ge_2Sb_2Te_5$ properties [9]. $Ge_2Sb_2Te_5$ exists in two phases: a metastable face-centered-cubic (FCC) structure, which forms at a temperature T~150°C [16], and a stable hexagonal structure, which forms above T~300°C [18]. In the FCC phase, a FCC sub-lattice containing only Te atoms (anion sites) is intercalated with another FCC sub-lattice containing a solid solution of Ge and Sb atoms as well as vacancies (cation sites). The amount of vacancies has been calculated to be a little less than 20% at [19]. In the hexagonal structure, atomic (basal) planes of Te atoms alternate with Ge and Sb planes [20].

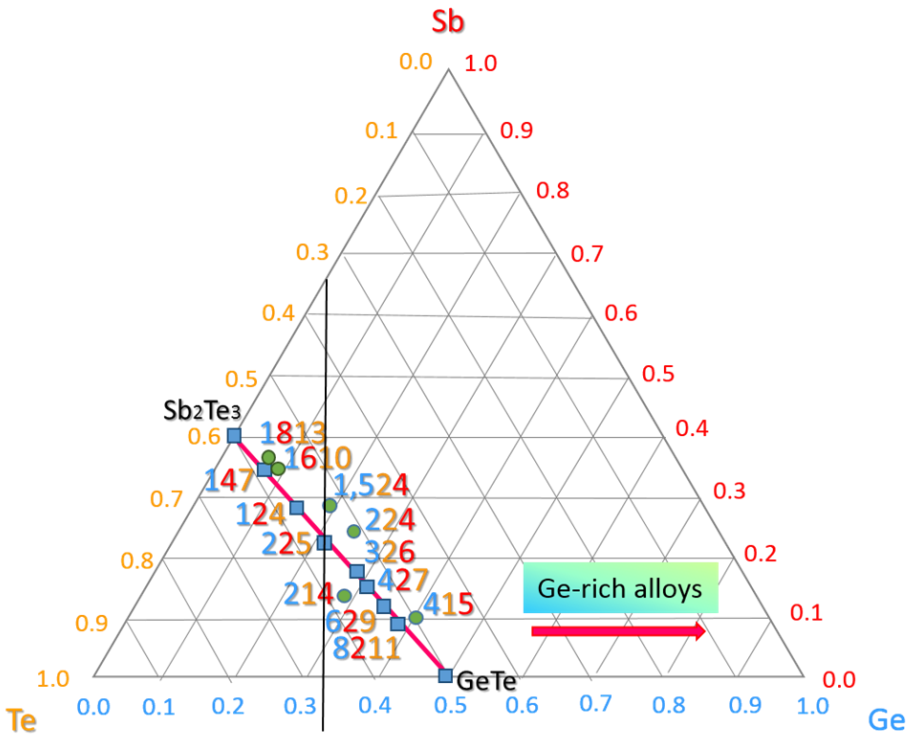

Fig. 1. Ternary phase diagram for GST compounds. The tie line is indicated in magenta color and intercepts the alloys exhibiting congruent melting. GST alloys such as $Ge_2Sb_2Te_5$, $GeSb_4Te_7$ [17], $GeSb_2Te_4$ [17], $Ge_3Sb_2Te_6$ [10], $Ge_4Sb_2Te_7$ [2,10], $Ge_6Sb_2Te_9$ [2], $Ge_8Sb_2Te_{11}$ [2] have been previously reported in literature and have been plotted here. Close to the tie line, Ge_4SbTe_5 [11,12], $GeSb_6Te_{10}$ [10], $GeSb_8Te_{13}$ [10], Ge_2SbTe_4 [14], $Ge_{1.5}Sb_2Te_4$ [14] and $Ge_2Sb_2Te_4$ [13,14] have also been reported. Ge-rich materials may be defined as those compounds which are located in the region right to the vertical black line passing through the $Ge_2Sb_2Te_5$ alloy.

Unfortunately, the crystallization temperature of $Ge_2Sb_2Te_5$ is not high enough to allow its use in several classes of applications (such as automotive and aerospace applications) where the device is exposed to temperatures higher than 150°C, thus inducing undesired phase transitions in the PCM. For some other applications, the information needs to be recorded before the soldering process, the latter being carried out at ~260°C, thus potentially altering the code integrity. Ge-rich GST materials have recently appeared as a good solution for PCM-based devices requiring elevate working temperatures [21,22]. Ge-rich GST materials usually refer to those compounds which contain more Ge than needed to satisfy the 225 stoichiometry. These compounds are located on the right of the $Ge_2Sb_2Te_5$ phase in the ternary phase diagram shown in Fig. 1. The performances of PCMs based on Ge-rich GST alloys have been also tested, demonstrating high data retention over an extended temperature range [23,24]. Moreover, N-doping has been shown to further increase the crystallization temperature, leading to better endurance, and to reduce the undesired drift phenomenon affecting the low resistance state [25-27].

Actually, the chemical compositions of these materials are defined in the "as-deposited" state and thus correspond to amorphous layers of homogeneous compositions. Whether or not these compositions and homogeneity remain unaltered during multiple cycling of a device and how the resulting structure can explain the observed properties are still open questions. In a PCM device, the amorphous-to-crystalline transition is promoted by electrical pulses which heat up a thin layer of GST material. Previous pioneering works have evidenced that chemical phase separation between Ge and some GST phase results from thermal annealing of full sheet deposited layers and from cycling of GST devices [23-26,28]. Nonetheless, an exhaustive analysis of the processes which take place during the crystallization of Ge-rich materials is still missing. While expected, the phase segregation probably occurring prior or during the crystallization of Ge-rich materials and the formation

of stable crystalline compounds have not been studied in detail. Unpredicted variations of the local composition of the material during cycling can represent a source of failure and compromise the memory device endurance [29,30]. It is thus of primary importance to investigate the changes of chemical composition which affect Ge-rich GST alloys during thermal annealing leading to their crystallization.

In this paper, we report a detailed study of the different and successive phenomena which take place during thermal annealing of a N-doped Ge-rich GST alloy. For this, we have studied thoroughly the structural and chemical characteristics of samples annealed at different and increasing temperatures. The microstructure of the layers was analyzed using Transmission Electron Microscopy (TEM) techniques and automated crystal orientation mapping (ASTAR), while their chemical composition was analyzed using high angle annular dark field scanning TEM (HAADF-STEM) imaging and STEM energy dispersive X-ray (STEM-EDX) mapping. We show that a chemically homogeneous amorphous Ge-rich GST material undergoes phase separation during annealing and finally transforms into a composite material based on the two most stable crystalline phases offered by the constituents, Ge and $Ge_2Sb_2Te_5$ crystals.

2. Experimental

A N-doped and highly Ge-enriched GST (E-GST, with [Ge] > 30%) film, with a thickness of 100 nm, was deposited by physical vapor deposition on a Si (100) substrate. Then, an ultra-thin (14 Å) Ti-rich TiN layer was deposited on the E-GST surface prior to the deposition of a 20 nm-thick TiN encapsulating layer. The wafer was cut into different samples and annealed in a horizontal Carbolite furnace under atmospheric pressure and N_2 flux, at different temperatures and times. In a previous paper [31] we have shown that the onset of the phase change occurs at temperature T~380°C. For this reason, thermal annealing were

performed at temperatures equal or larger than 380°C, i.e. at 380°C for 1 hour, 400°C for 30 minutes, 450°C for 30 minutes and 500°C for 30 minutes. TEM specimens were prepared in cross-section by traditional mechanical polishing followed by ion beam thinning (as-deposited, annealed 380°C/1 hour and annealed 400°C/30 minutes samples) or by focus ion beam (FIB) techniques (annealed 450°C/30 minutes. and 500°C/30 minutes specimens). The use of FIB for these latter samples annealed at higher temperatures was required due to the formation of blisters on the surface of these samples during annealing, which hampers the bonding of two samples face to face. A scanning electron microscope (SEM) image of these blisters is provided in the supporting information, Fig. S1(a). To understand the origin of these blisters, a FIB lamella was prepared at the edge of such a blister [Fig. S1(a)]. TEM analyses on this sample [Fig. S1(b)] revealed that the blisters are formed from the exfoliation of the TiN layer. Based on our experience [32], we believe that the blisters form as a result of N-exodiffusion from the E-GST film and N_2 gas accumulation and pressurization below the TiN layer during high enough temperature annealing. Specimen preparation and SEM analyses were carried out using a FEI Helios Nanolab 600 dual-beam FIB and SEM. TEM conventional imaging, selected area electron diffraction (SAED), high resolution TEM (HRTEM) and HAADF-STEM analyses were performed using an aberration corrected FEI TECNAIF20, equipped with a FEG source. STEM-EDX and ASTAR (TEM orientation imaging) analyses were performed using a Philips CM20-FEG TEM. STEM-EDX analyses were performed using a Microanalyser QUANTAX XFlash detector with a 30 mm^2 active area and an energy resolution of 127 eV, while EDX quantification was performed by exploiting the Esprit 1.9 software. ASTAR imaging was performed using the Nanomegas Digistar ACOM system [33].

3. Results

Figure 2(a) shows a bright field (BF) TEM image of the as-deposited E-GST film. The polycrystalline TiN encapsulating layer is well distinguishable on top of the GST. The uniform contrast across the E-GST layer and the halo observed in the associated diffraction pattern, shown in the inset of Fig. 2(a), indicate that, as deposited, the E-GST material is in an amorphous phase. The bright spots visible in the diffraction pattern correspond to the crystal planes of TiN, which is polycrystalline. STEM-EDX analyses were performed on this as-deposited E-GST in order to examine the chemical composition across the film. STEM-EDX maps are displayed in Fig. 2(b-f) for each chemical element composing the film, namely Ge [Fig. 2(b)], Sb [Fig. 2(c)], Te [Fig. 2(d)] and N [Fig. 2(e)]. The native Si oxide layer is detected at the interface between the Si substrate and the E-GST, as shown in Fig. 2(f). From the quantitative analysis of each STEM-EDX map, it can be inferred that the atomic composition of the as-deposited E-GST film is homogeneous across the GST layer.

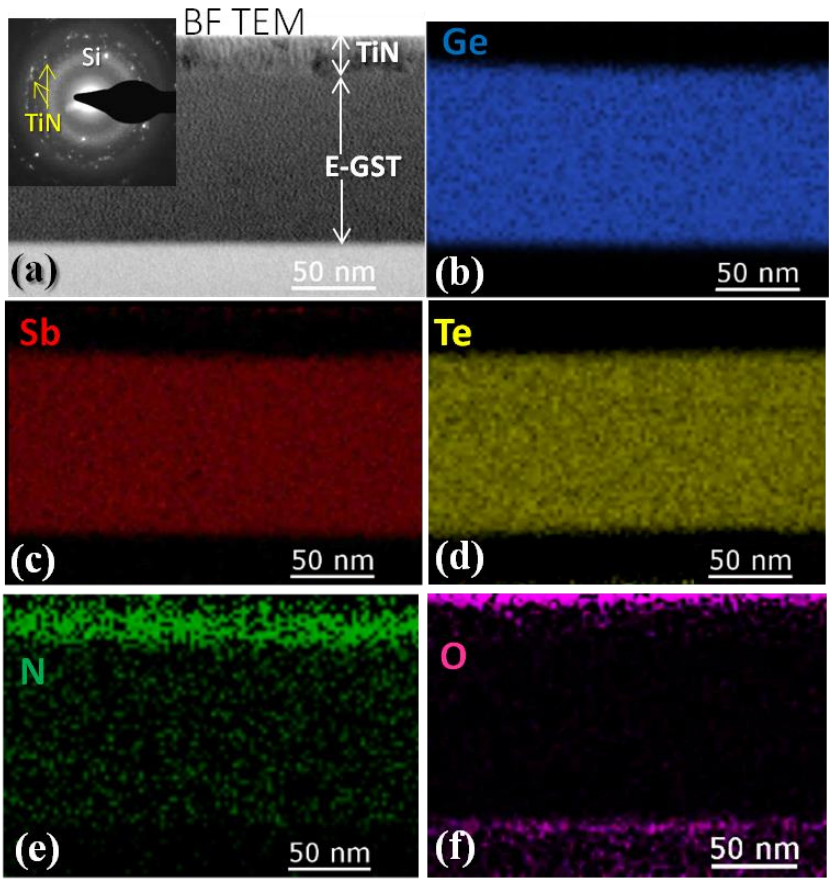

Fig. 2. (a) BF-TEM image of as-deposited E-GST and its SAED in the inset. The chemical composition is homogeneous across the film, as evidenced by the STEM-EDX maps of (b) Ge, (c) Sb, (d) Te, (e) N. The presence of a thin Si oxide layer at the Si/E-GST interface is evidenced in (f).

Figure 3(a) shows a BF-TEM image of the sample annealed at 380°C for 1 hour. The image contrast is no more homogeneous across the layer. Bright zones of nanometric dimensions are detected, surrounded by a darker matrix. This contrast does not change with the specimen orientation. Interestingly, the associated SAED pattern, shown in the inset of Fig. 3(a), only reveals the diffuse halo characteristic of the amorphous phase of E-GST and the rings characteristic of the polycrystalline TiN top layer. Thus, it is suspected that the contrast in the BF image results from density variations i.e., local variations of the chemical composition, and not from diffraction effects revealing the nucleation of a crystalline phase. To confirm this finding, HAADF-STEM imaging of the same specimen was performed. Such an image is shown in Fig. 3(b).

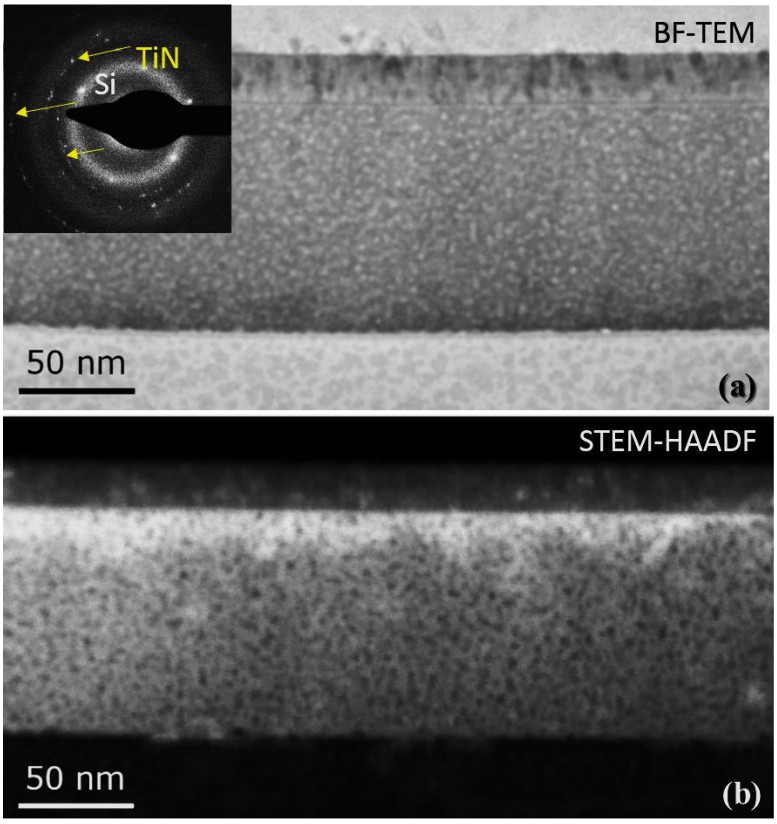

Fig. 3. (a) BF-TEM image and (b) HAADF-STEM image of E-GST annealed at 380°C for 1 hour, both showing the same nanometric contrast. The SAED shown in the inset of (a) indicates that the film is in the amorphous state.

In HAADF-STEM imaging, the Rutherford-scattering of electrons is maximized and diffraction-contrast effects are smoothed out. Since the Rutherford cross-section is proportional to Z^2 (where Z is the atomic number), the contrast of HAADF-STEM images is related to differences of the mean atomic number from one region to the other and hence to the local material composition [34]. In Fig. 3(b), we again note the same nanometric "objects" as those observed in BF-TEM, but this time they appear in black. This evidences that they originate from regions of smaller atomic density. Finally, the contrasts observed both in the BF-TEM and the HAADF-STEM images evidence that annealing at 380°C for one hour results in fluctuations of the chemical composition of the material and this while staying in the amorphous phase.

We consider afterwards the E-GST annealed at 400°C for 30 minutes. A typical BF-TEM image of this sample is shown in Fig. 4(a) along with its associated SAED pattern in

Fig. 4(b). As discussed in our previous work [31], this pattern evidences the coexistence of two crystalline phases which sequentially form during annealing: cubic Ge and FCC-GST. Since the structure of FCC-GST crystals only marginally varies with stoichiometry along the congruent line, the exact composition of these GST crystals cannot be inferred from such diffraction patterns. The BF-TEM image shows the presence of very small crystals (3 nm, as indicated by the red arrow in Fig. 4(a)) as well as larger crystalline regions (dimensions of ~30 nm) in the layer. HRTEM images, as the one shown in the inset of Fig. 4(a), reveal that the small crystalline grains are interspersed within some amorphous phase.

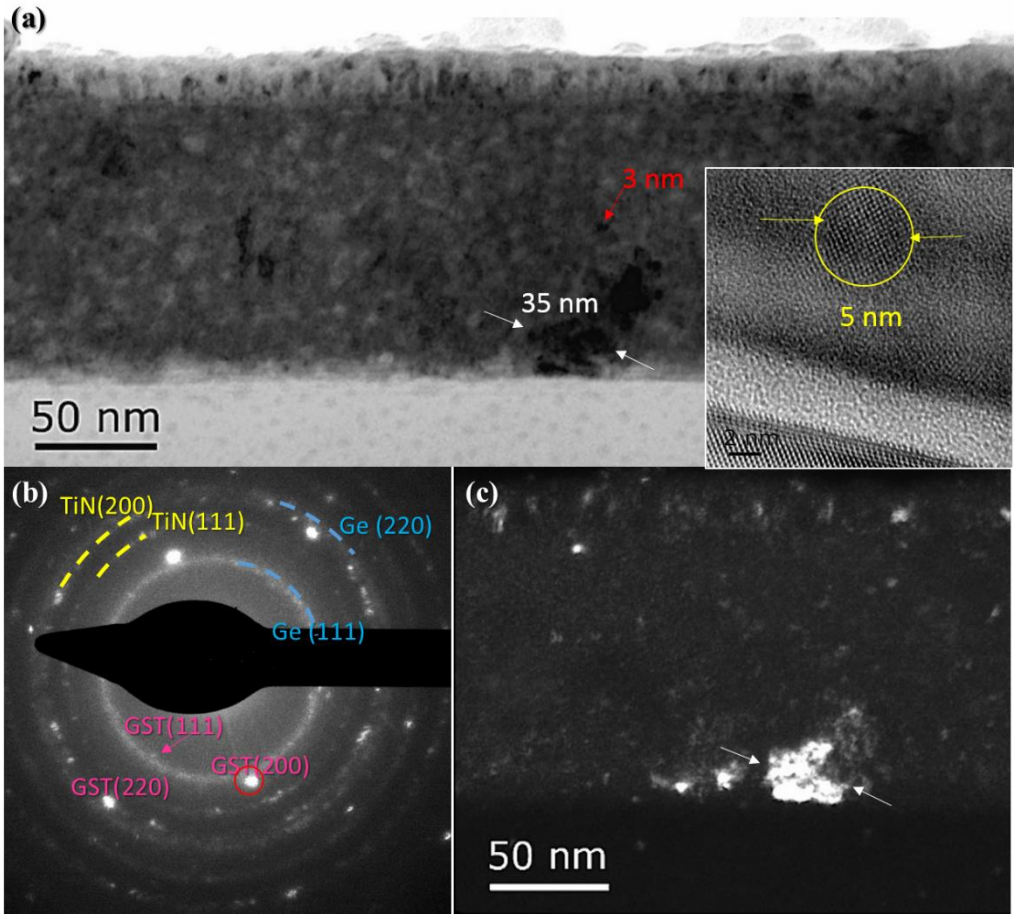

Fig. 4. (a) BF-TEM image of the E-GST annealed at 400°C for 30 minutes and (b) the corresponding SAED. (c) DF image obtained by selecting the diffraction spot indicated by the red circle. A typical HRTEM image of this sample is also shown in the inset of (a).

The structural characteristics of the small crystals and of the larger crystalline regions have been further studied using dark field (DF) imaging. Figure 4(c) is a DF image obtained by selecting the GST spot in the SAED pattern, as indicated by the red circle in Fig. 4(b). As this spot is very close to the diffraction ring characteristic of the Ge phase, the DF image results from both contributions. Under such conditions, the images show faintly visible small nanocrystals homogeneously dispersed across the E-GST layer and larger and defective crystalline regions of irregular shapes.

Figure 5(a) shows the BF-TEM image of one of these large crystalline regions. Figure 5(b) is the corresponding DF image taken by selecting the FCC-GST diffraction spot, while Fig. 5(c) is taken by selecting electrons originating from the Ge ring but far from any FCC-GST spot. The contrast seen in these images clearly evidences that the small crystals are made of Ge while the large crystalline regions are made of FCC-GST.

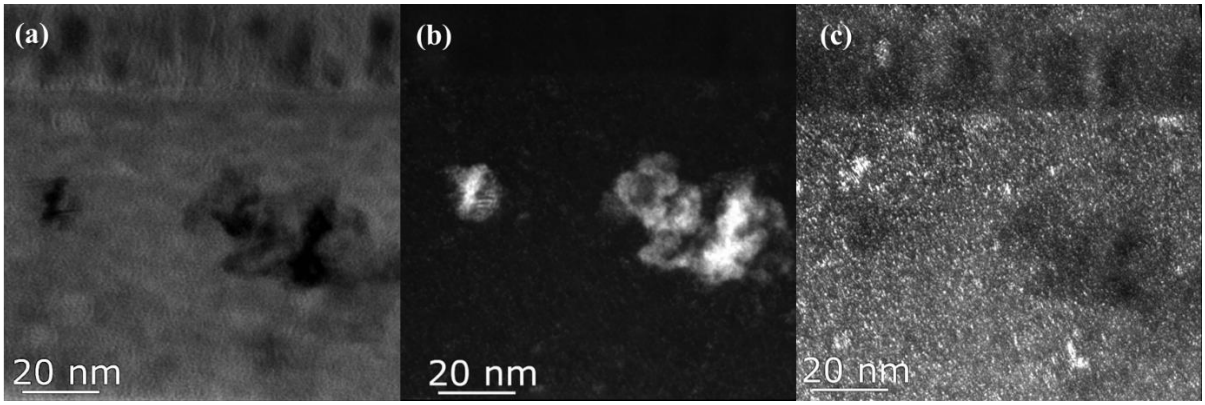

Fig. 5. (a) BF-TEM image showing a crystalline region in E-GST annealed at 400°C. The corresponding DF images taken (b) by selecting the FCC-GST diffraction spot and (c) along the Ge ring are also shown.

To confirm our findings, we have analyzed the composition of these films using STEM-EDX. Figure 6(a-f) is a set of STEM-EDX maps taken on the same sample and showing the spatial distribution of the elements within the layer. While nitrogen is still homogenously distributed across the layer, Ge, Te and, to a lesser extent, Sb have been redistributed during annealing.

Clearly, there exist regions, typically of several tens of nanometers wide, which are Ge-depleted while they show an increased concentration of Te. The Sb map, although less contrasted, shows the same features than the Te map. This set shows that amorphous homogeneous Ge-rich GST undergoes some phase separation during annealing at 400°C [28].

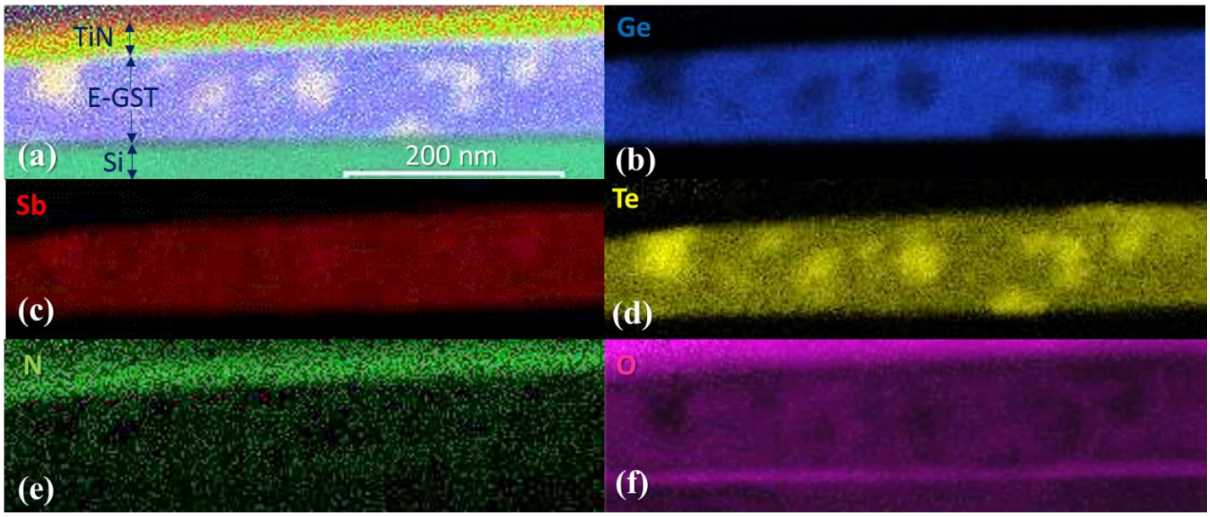

Fig. 6. (a) Superposition of the STEM-EDX maps of (b) Ge, (c) Sb, (d) Te, (e) N and (f) O relatively to E-GST annealed at 400°C for 30 minutes.

Interestingly, oxygen, which was present only above the TiN cap layer and at the Si/GST interface (native Si oxide) has diffused and tends to accumulate in the Ge-rich zones [Fig. 6(f)].

Figure 7(a) is a typical BF-TEM image of the layer annealed at 450°C for 30 minutes. The whole layer consists of a mixture of few large (typically from 30 to 70 nm) crystalline regions surrounded by numerous but smaller (5-10 nm) grains. Typical HRTEM images, such as the one displayed in Fig. 7(b), evidence the co-existence of pure Ge and GST crystals.

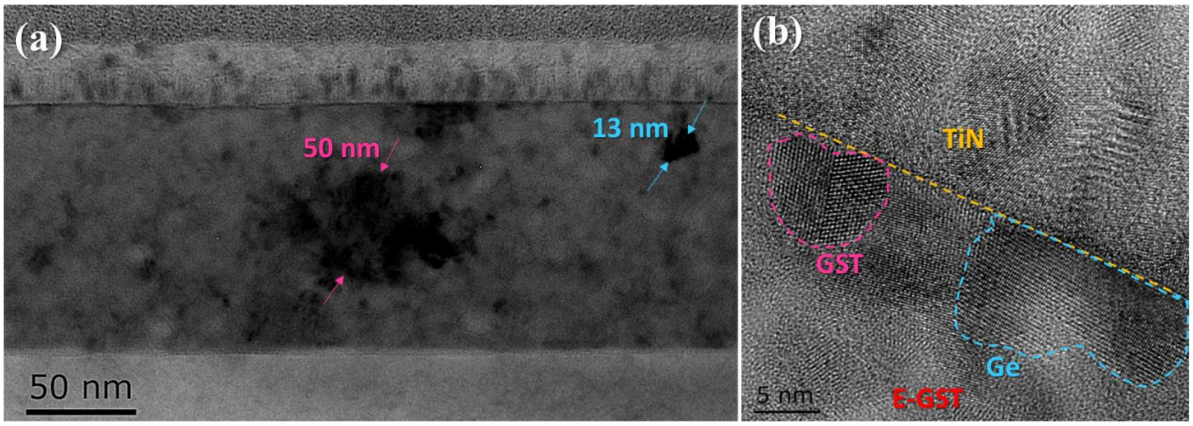

Fig. 7. (a) BF-TEM image of the E-GST annealed at 450°C for 30 minutes. (b) Typical HRTEM image of the same sample.

Careful analysis using DF images selecting either a diffraction spot characteristic of the Ge or of the GST phase unambiguously shows again that the larger crystalline regions have the GST structure while the smallest ones are of pure cubic Ge [Fig. 8(a-d)]. Moreover, it is clear that both the Ge and the GST grains are larger after annealing at 450°C for 30 minutes than after annealing at 400°C for the same time interval.

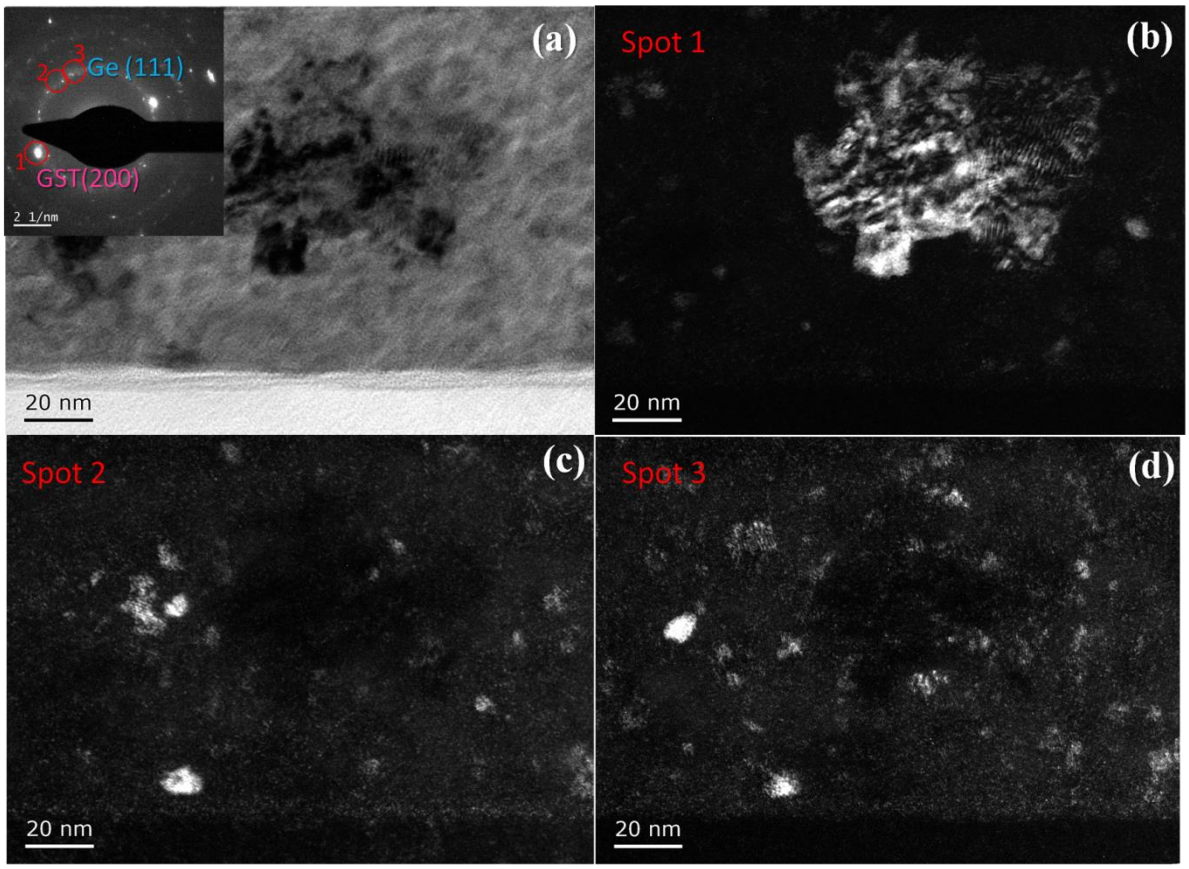

Fig. 8. (a) BF image of a crystalline zone of E-GST annealed at 450°C for 30 minutes and its SAED in the inset. (b-d) Series of DF images.

Figure 9(a-f) shows the chemical mapping obtained by STEM-EDX on this sample. Compared to those shown in Fig. 6, these maps show that the Te and Sb-rich regions are now larger in size and that the contrast between the Ge-rich and Te-rich regions is higher. This indicates that phase separation continued during annealing at 450°C and led to the growth of the two types of regions we have evidenced. The oxygen map also confirms that oxygen has largely redistributed from the Si/E-GST interface towards the layer and preferentially getters in the Ge-rich regions.

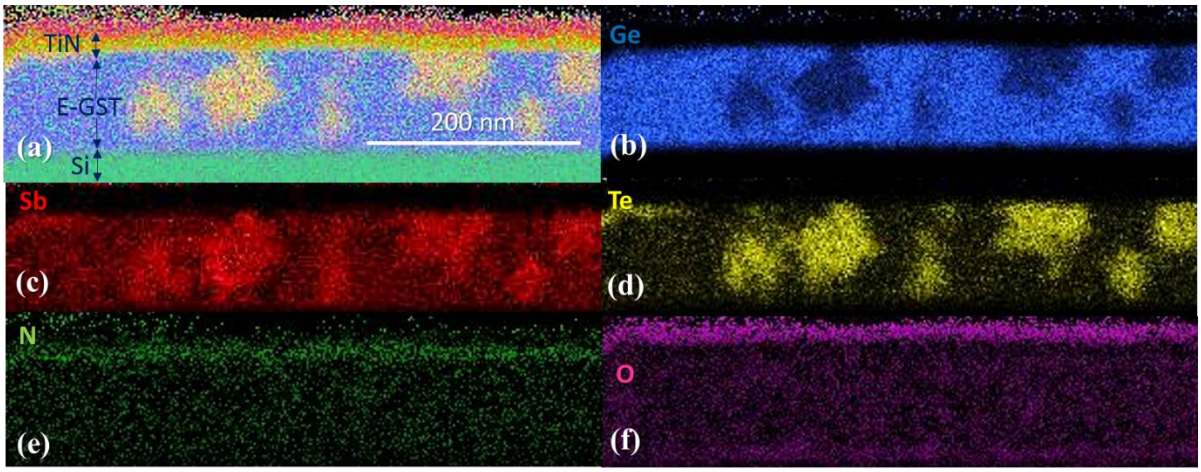

Fig. 9. (a) Superposition of the STEM-EDX maps of (b) Ge, (c) Sb, (d) Te, (e) N and (f) O relatively to E-GST annealed at 450°C for 30 minutes.

At this stage, it is very tempting to try to deduce the actual composition of the grains showing the FCC-GST structure from the STEM-EDX data. This would require that different grains do not overlap in the image i.e., that the specimen thickness is equal or smaller than the grain size. This has been achieved on samples annealed at 500°C for 30 minutes.

Figure 10(a) shows a BF-TEM image of this sample. After such an annealing, the layer consists of a mixture of large crystals and voids, as previously noticed by Padilla et al. [29]. The associated SAED pattern shows well defined spots corresponding to the cubic Ge and FCC-GST structure. HRTEM imaging [Fig. 10(b)] shows that the very large crystals have the FCC-GST (not hexagonal) structure and contain only few defects.

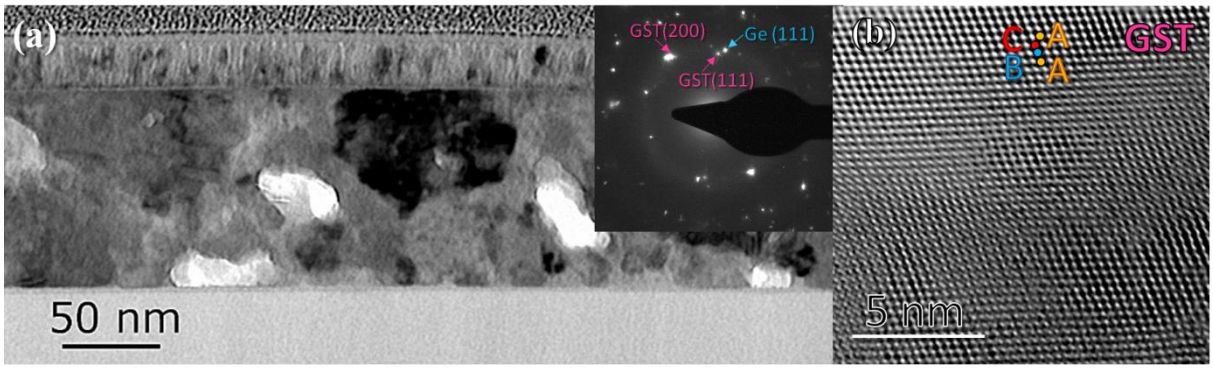

Fig. 10. (a) BF-TEM image of E-GST annealed at 500°C for 30 minutes and its SAED in the inset. (b) HRTEM of a large GST crystal: the stacking sequence abcabc… evidences the cubic structure.

ASTAR imaging was used to provide orientation mapping of the different crystals found in the sample annealed at 500°C for 30 minutes. This technique is based on a collection of precession electron diffraction patterns acquired at each point by scanning the electron beam over the sample. In our case, each acquired electron diffraction pattern was compared numerically with those theoretically corresponding to pure Ge and $Ge_2Sb_2Te_5$. The resulting ASTAR map is shown in Fig. 11(a) and displays large $Ge_2Sb_2Te_5$ crystals in yellow surrounded by Ge crystals in blue. This analysis firstly shows that, after annealing at 500°C for 30 minutes, the E-GST is fully crystallized. However, since the structures corresponding to the different GST materials lying on the congruent line shown in Fig.1 cannot be sorted out based only on their diffraction patterns, one cannot conclude on which GST alloy has crystallized. For this reason, we have investigated the chemical composition of the GST grains using STEM-EDX on the same region of the sample imaged by ASTAR. Chemical maps are shown in Fig.11(b-g). The contrast between the Ge-rich and the Te and Sb-rich regions is very high. This is due from one hand to the thin thickness of the sample but also to the full separation of the two Ge and GST phases. Comparing these chemical maps with the ASTAR image of Fig. 11(a), one can see that the initially homogeneous layer has transformed into a layer of 50-100 nm wide GST crystals embedded in a Ge crystalline matrix.

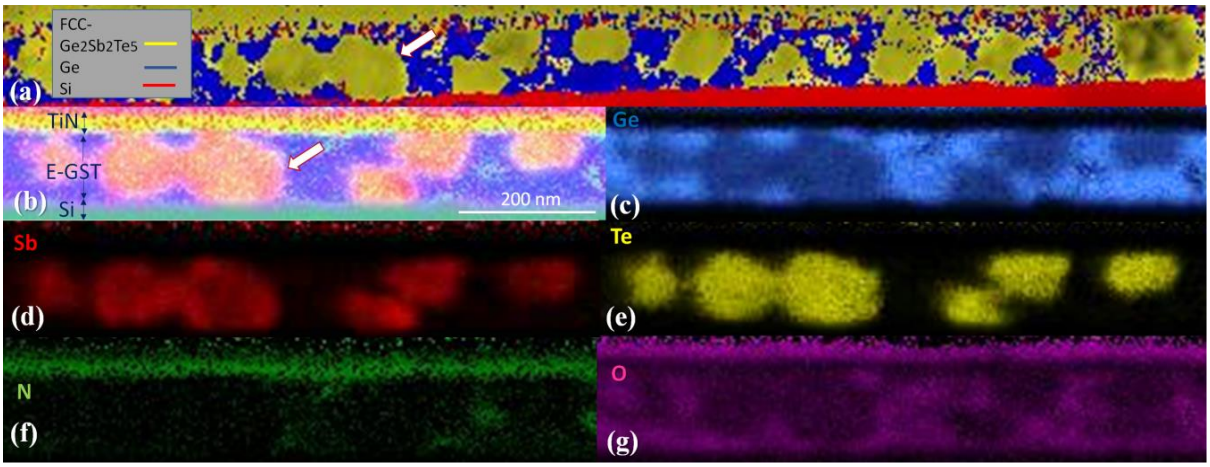

Fig. 11. (a) ASTAR map of the E-GST annealed at 500°C for 30 minutes. (b) Superposition of the STEM-EDX maps of (c) Ge, (d) Sb, (e) Te, (f) N and (g) O relatively to the same sample. As a reference, the arrows in (a) and (b) indicate the same crystal.

As said above, since there is little overlap between the Ge matrix and the GST crystals in the sample annealed at 500°C for 30 minutes, STEM-EDX can be used to measure locally, on specific grains, the actual composition of the GST crystals. The ratios Ge/Te, Sb/Te and Ge/Sb can be used to infer its stoichiometry, as long as Te atoms are located only on the anionic sites, while the cationic sites can host Ge, Sb atoms or vacancies in different proportions which define the actual stoichiometry of the GST alloy. Table 1 shows the ratios which are expected for the different known phases of GST. Table 2 reports the experimental values we have measured on the different GST grains found in the film annealed at 500°C for 30 minutes. The experimental error is also reported.

Table 1. Ge/Te, Sb/Te and Ge/Sb characteristic ratios of the different GST phases shown in Fig.1.

GST Stoichiom.	Ge/Te	Sb/Te	Ge/Sb
2-2-5	0,4	0,4	1,0
1-8-13	0,1	0,6	0,1
1-6-10	0,1	0,6	0,2

1-4-7	0,1	0,6	0,3
1-2-4	0,3	0,5	0,5
1.5-2-4	0,4	0,5	0,8
3-2-6	0,5	0,3	1,5
4-2-7	0,6	0,3	2,0
2-1-4	0,5	0,3	2,0
6-2-9	0,7	0,2	3,0
8-2-11	0,7	0,2	4,0
4-1-5	0,8	0,2	4,0

Table 2. Ge/Te, Sb/Te and Ge/Sb ratios measured by quantitative STEM-EDX analysis on the different GST grains observed in the ASTAR and STEM-EDX maps shown in Fig. 11, corresponding to the sample annealed at 500°C for 30 minutes.

	Ge/Te	$\sigma_{(Ge/Te)}$	Sb/Te	$\sigma_{(Sb/Te)}$	Ge/Sb	$\sigma_{(Ge/Sb)}$
Crystal-1	0,5	0,3	0,5	0,2	1,0	0,7
Crystal-2	0,6	0,3	0,7	0,3	0,8	0,5
Crystal-3	0,6	0,3	0,7	0,3	0,9	0,5
Crystal-4	0,7	0,3	0,6	0,3	1,0	0,7
Crystal-5	0,8	0,3	0,5	0,2	2	1
Crystal-6	0,8	0,4	0,7	0,3	1,1	0,7
Crystal-7	0,7	0,3	0,6	0,3	1,2	0,8
Crystal-8	0,7	0,3	0,5	0,2	1,3	0,9
Crystal-9	0,8	0,4	0,7	0,3	1,2	0,8
Crystal-10	0,7	0,3	0,6	0,3	1,1	0,7

First, the Ge/Sb ratio which is experimentally measured most often close to 1 allows one to rule out a large number of GST stoichiometries. In particular, Ge-rich GST phases do not fulfill this criterion. The well-known 225 stoichiometry provides a better agreement although the larger than predicted Ge/Te and Sb/Te ratios we have measured may be an indication that some of the vacancies normally sitting on the cationic sub-lattice have been filled with Ge and Sb atoms.

4. Discussion

Summarizing our results, we have evidenced that homogeneous Ge-rich GST alloys are stable up to 380°C. At this temperature, chemical inhomogeneities (Ge-rich, Ge-poor) at the nanoscale start to appear while the material is still in the amorphous phase. Ge atoms diffuse and segregate in regions of nanometric dimensions. The nucleation of pure Ge nanocrystals occurs only after longer annealing times, once this phase separation has been consolidated [31]. Annealing at 400°C favors this segregation further and allows the crystallization of two phases: large (several tens of nanometers) crystals exhibiting a cubic GST structure are found, surrounded by a high density of cubic Ge nanocrystals, as also reported previously by Privitera et al. [28]. Annealing at 450°C results into an increase of the sizes of both types of crystals. Finally, after annealing at 500°C, the layer is totally crystalline. In general, the GST crystals are large (up to one hundred of nanometers), surrounded and isolated from each other by a matrix of Ge nanocrystals. Interestingly, these Ge grains appear to have gettered the oxygen atoms initially present in the native oxide at the Si/E-GST interface.

Quantitative chemical analysis shows that the material has transformed into two pure and well identified phases, the cubic Ge and a cubic GST phase, most probably, the FCC-

$Ge_2Sb_2Te_5$. However, the Ge/Te and Sb/Te ratios we have measured, slightly larger than expected for a regular $Ge_2Sb_2Te_5$, might indicate that this material is doped, with Ge and Sb atoms at sites normally vacant on the cationic lattice (20%). It is important to note that, despite the high temperature involved, the GST phase we evidence is still cubic, as demonstrated by the HRTEM images, and not hexagonal as expected after annealing above the cubic-to-hexagonal transition temperature of the $Ge_2Sb_2Te_5$ i.e., 300-350°C [18]. It is thus suspected that this transition is hampered by the environment, the Ge phase and probable stress at the interfaces. However, it is not unreasonable to think that the delicate balance between Ge and Sb atoms and vacancies on the same sub-lattice may be affected by such strong out-of-equilibrium conditions (more than 150°C above the transition temperature). The observation of voids, precipitates of vacancies, in the layer reveals that, at some point, the crystals have expulsed vacancies, in support of our hypothesis for a "doped" $Ge_2Sb_2Te_5$ phase.

Most importantly, our results show that the crystallization of a Ge-rich GST material proceeds through different steps. First, chemical fluctuations of the initially homogeneous amorphous phase take place, driven by Ge diffusion, and lead to Ge segregation. Then, Ge crystallization occurs and forms Ge nanocrystals. The observation of oxygen gettering on these nanocrystals, probably on their facets, may explain why they do not grow so much in size but instead stay small and nucleate in huge density. Once these crystals are formed, they drive Ge diffusion from the surrounding matrix towards them, hence decreasing the Ge concentration in the matrix. Experimentally, it is only after many Ge nanocrystals have been formed that the first GST crystals nucleate. This observation strongly suggests that a too high local concentration of Ge hampers the crystallization of the GST phase. In other words, the Ge concentration increases the energy barrier height for the amorphous to crystalline

transition of GST. It is only after a region has been “purified” from Ge that it can crystallize as a GST phase.

All our observations support the idea that the change of properties which are sought for memory applications i.e., higher thermal stability and increase of “transition temperature”, are not intrinsic properties of some precise Ge-rich phases, but result from kinetic factors. Indeed, phase segregation phenomena are energetically expensive processes which involve long range diffusion of atomic species, what explains the need for longer incubation times for crystallization as well as higher thermal stability of the amorphous phase when the Ge content is increased.

While selecting doped GST alloys on the basis of the classical graphs showing the variations of the resistivity as a function of the annealing temperature is certainly pertinent for enlarging the application domains of PCMs [23-25], our results show that Ge-rich alloys decompose and crystallize as a two-phase material. Thus, such graphs evidences that, given the volume of material probed by the measurement and the annealing ramp-up rate, the time spent at some temperature and below was sufficient for the system to undergo phase separation between Ge and $Ge_2Sb_2Te_5$.

5. Conclusion

Using a variety of TEM based techniques, we have investigated the changes which affect the structure and composition of Ge-rich GST alloys during thermal annealing. We show that, although Ge-rich GST materials can be grown as amorphous layers of homogeneous compositions, the primary effect of annealing is to activate phase separation between stable Ge and GST phases. This phase separation starts at 380°C while the material is still amorphous. and later leads to the nucleation of the first Ge nanocrystals. Increasing the

annealing temperature to 400 and then 450°C allows the crystalline Ge phase to grow by driving the excess Ge out of the matrix and finally to the formation of large (30-50 nm) crystals with the FCC-GST structure. After annealing at 500°C for 30 minutes, the layer has fully crystallized and consists of a population of large (50-100 nm) FCC-GST crystals with a stoichiometry close to 225 buried in a matrix composed of small Ge nanocrystals.

This study evidences that the superior properties of Ge-rich alloys i.e., higher thermal stability and larger crystallization temperature, do not result from the intrinsic properties of some Ge-rich crystalline phase but from kinetic factors, and involves long range diffusion of atomic species, first and foremost Ge. The crystallization kinetics of such two-phase materials is diffusion limited and requires adequate combinations of temperatures and times to occur.

Acknowledgements

The authors would like to thank the people in charge of the TEM and FIB facility at CEMES, in particular C. Marcelot and R. Cours for their precious technical support. This work was partially funded by Minefi through the Nano2017 initiative and by the Labex NEXT (n° ANR-10-LABX-0037) in the framework of the “Programme des Investissements d'Avenir”.

References

[1] G. W. Burr, M. J. Breitwisch, M. Franceschini, D. Garetto, K. Gopalakrishnan, B. Jackson, B. Kurdi, C. Lam, L. A. Lastras, A. Padilla, B. Rajendran, S. Raoux, R. S. Shenoy, Phase change memory technology, J. Vac. Sci. Technol. B 28 (2010) 223-262.

[2] M. Wuttig, N. Yamada, Phase-change materials for rewriteable data storage, Nature Mater. 6 (2007) 824-832.

[3] W. Wełnic, M. Wuttig, Reversible switching in phase-change materials, Mater. Today 11 (2008) 20-27.

[4] G. W. Burr, M. J. Brightsky, A. Sebastian, H.-Y. Cheng, J.-Y. Wu, S. Kim, N. E. Sosa, N. Papandreou, H.-L. Lung, H. Pozidis, E. Eleftheriou, C. H. Lam, Recent Progress in Phase-Change Memory Technology, IEEE Trans. Emerg. Sel. Topics Circuits Syst. 6 (2016) 146-162.

[5] T. Nirschl, J. B. Philipp, T. D. Happ, G. W. Burr, B. Rajendran, M.-H. Lee, A. Schrott, M. Yang, M. Breitwisch, C.-F. Chen, E. Joseph, M. Lamorey, R. Cheek, S.-H. Chen, S. Zaidi, S. Raoux, Y.C. Chen, Y. Zhu, R. Bergmann, H.-L. Lung, C. Lam, Write Strategies for 2 and 4-bit Multi-Level Phase-Change Memory, Tech. Dig. - Int. Electron Devices Meet. 17.5. (2007) 461-464.

[6] F. Bedeschi, R. Fackenthal, C. Resta, E. M. Donze, M. Jagasivamani, E. C. Buda, F. Pellizzer, D. W. Chow, A. Cabrini, G. Calvi, R. Faravelli, A. Fantini, G. Torelli, D. Mills, R. Gastaldi, G. Casagrande, A Bipolar-Selected Phase Change Memory Featuring Multi-Level Cell Storage, IEEE J. Solid-State Circuits 44 (2009) 217-227.

[7] G. H. Oh, Y. L. Park, J. I. Lee, D. H. Im, J. S. Bae, D. H. Kim, D. H. Ahn, H. Horii, S.O. Park, H. S. Yoon, I. S. Park, Y. S. Ko, U-in Chung, J.T. Moon, Parallel multi-conned (PMC) cell technology for high density MLC PRAM, Symposium on VLSI Technology (2009) 220-221.

[8] A. Gyanathan, Y. C. Yeo, Two-bit multi-level phase change random access memory with a triple phase change material stack structure, J. Appl. Phys. 112 (2012) 104504.

[9] J.-C. Bastien, Etude des matériaux à changement de phase pour application dans le domaine des PCRAM-Verres infrarouges pour l'optique spatiale, PhD thesis, Université de Rennes 1 (2011).

[10] L. E. Shelimova, O. G. Karpinskii, P. P. Konstantinov, M. A. Kretova, E. S. Avilov, V. S. Zemskov, Composition and Properties of Layered Compounds in the GeTe–Sb2Te3 System, Inorg. Mater. 37 (2001) 342–348.

[11] H.-W. Woltgens, R. Detemple, I. Friedrich, W. K. Njoroge, I. Thomas, V. Weidenhof, S. Ziegler, M. Wuttig, Exploring the limits of fast phase change materials, Mat. Res. Soc. Symp. Proc. 674 (2001) V1.3.1- V1.3.6.

[12] D. Wamwangi, W. K. Njoroge, M. Wuttig, Crystallization kinetics of Ge4Sb1Te5 films, Thin solid films 408 (2002) 310-315.

[13] W. Wetnic, D. Lusebrink, D. Wamwangi, M. Gilleßen, R. Dronskowski, M. Wutting, Controlling Material Properties in new Phase Change Alloys beyond the pseudobinary line, available at: https://www.researchgate.net/publication/255628768_Controlling_Material_Properties_in_new_Phase_Change_Alloys_beyond_the_pseudobinary_line.

[14] W. Wełnic, J. A. Kalb, D. Wamwangi, C. Steimer, M. Wuttig, Phase change materials: From structures to kinetics. J. Mater. Res. 22(9) (2007) 2368-2375.

[15] J. Van Eijk, P. Merkelbach, C. Braun, D. Lencer, W. Bensch, M. Wuttig, Investigation of local distortions in the rocksalt structure of Ge2Sb2Te4, available at http://hasyweb.desy.de/science/annual_reports/2007_report/part1/contrib/41/21048.pdf.

[16] N. Yamada, E. Ohno, K. Nishiuchi, N. Akahira, M. Takao, Rapid-phase transitions of GeTe-Sb2Te3 pseudobinary amorphous thin films for an optical disk memory, J. Appl. Phys. 65 (1991) 2849–2856.

[17] N. K. Abrikosov, G.T. Danilova-Dobryakova, An investigation of the structural diagram of Sb2Te3-GeTe, Izv. Akad. Nauk.SSR Neorg. Mater.1 (1965) 204-207.

[18] Y. Zheng, Y. Cheng, R. Huang, R. Qi, F. Rao, K. Ding, W. Yin, S. Song, W. Liu, Z. Song, S. Feng, Surface Energy Driven Cubic-to-Hexagonal Grain Growth of Ge2Sb2Te5 Thin Film, Sci. Rep. 7 (2017) 5915.

[19] N. Yamada, T. Matsunaga, Structure of laser-crystallized sputtered thin films for use in optical memory, J. Appl. Phys. 88 (2000) 7020-7028.

[20] T. Matsunaga, N. Yamada, Y. Kubota, Structures of stable and metastable Ge2Sb2Te5, an intermetallic compound in GeTe-Sb2Te3 pseudo-binary systems, Acta Crystallogr. Section B B60 (2004) 685–691.

[21] M. Aoukar, Dépôt de matériaux à changement de phase par PE-MOCVD à injection liquide pulsée pour des applications mémoires PCRAM, PhD thesis, Université de GRENOBLE ALPES (2015).

[22] M. Coué, Electrical characterization & TEM analyses of the physical mechanisms governing reliability of Ge-rich Phase-Change Memories, PhD thesis, Université de GRENOBLE ALPES (2016).

[23] V. Sousa, G. Navarro, N. Castellani, M. Coué, O. Cueto, C. Sabbione, P. Noé, L. Perniola, S. Blonkowski, P. Zuliani, R. Annunziata, Operation fundamentals in 12Mb Phase Change Memory based on innovative Ge-rich GST materials featuring high reliability performance, Symp. on VLSI Tech. Dig. IEEE (2015) 98-99.

[24] P. Zuliani, E. Varesi, E. Palumbo, M. Borghi, I. Tortorelli, D. Erbetta, G. Dalla Libera, N. Essina, A. Gandolfo, C. Prelini, L. Ravazzi, R. Annunziata, Overcoming temperature limitations in phase change memories with optimized GexSbyTez, IEEE Trans. Electron Devices 60 (2013) 4020-4026.

[25] G. Navarro, M. Coué, A. Kiouseloglou, P. Noé, F. Fillot, V. Delaye, A. Persico, A. Roule, M. Bernard, C. Sabbione, D. Blachier, V. Sousa, L. Perniola, S. Maitrejean, A. Cabrini, G. Torelli, P. Zuliani, R. Annunziata, E. Palumbo, M. Borghi, G. Reimbold, B. De Salvo, Trade-off Between SET and Data Retention Performance Thanks to Innovative Materials for Phase-Change Memory, Tech. Dig. - Int. Electron Devices Meet. (2013) 21.5.1–21.5.4.

[26] G. Navarro, V. Sousa, P. Noé, N. Castellani, M. Coué, J. Kluge, A. Kiouseloglou, C. Sabbione, A. Persico, A. Roule, O. Cueto, S. Blonkowski, F. Fillot, N. Bernier, R. Annunziata, M. Borghi, E. Palumbo, P. Zuliani and L. Perniola, N-doping Impact in Optimized Ge-rich Materials Based Phase-Change Memory, 2016 IEEE 8th International Memory Workshop (2016) 1-4.

[27] A. Kiouseloglou, G. Navarro, V. Sousa, A. Persico, A. Roule, A. Cabrini, G. Torelli, S. Maitrejean, G. Reimbold, B. De Salvo, F. Clermidy, L. Perniola, A Novel Programming Technique to Boost Low-Resistance State Performance in Ge-Rich GST Phase Change Memory, IEEE Trans. Electron Devices 61 (2014) 1246.

[28] S. M. S. Privitera, V. Sousa, C. Bongiorno, G. Navarro, C. Sabbione, E. Carria, E. Rimini, Atomic diffusion in laser irradiated Ge rich GeSbTe thin films for phase change memory applications, J. Phys. D: Appl. Phys. 51 (2018) 145103.

[29] A. Padilla, G. W. Burr, C. T. Rettner, T. Topuria, P. M. Rice, B. Jackson, K. Virwani, A. J. Kellock, D. Dupouy, A. Debunne, R. M. Shelby, K. Gopalakrishnan, R. S. Shenoy, B. N. Kurdi, Voltage polarity effects in Ge2Sb2Te5-based phase change memory devices, J. Appl. Phys. 110 (2011) 054501.

[30] L. Crespi, A. Lacaita, M. Boniardi, E. Varesi, A. Ghetti, A. Redaelli, G. D'Arrigo, Modeling of atomic migration phenomena in phase change memory devices, Proc. 2015 IEEE Int. Memory Workshop (2015) 1–4.

[31] M. Agati, F. Renaud, D. Benoit, A. Claverie, In-situ transmission electron microscopy studies of the crystallization of N-doped Ge-rich GeSbTe materials, MRS Comm. 8 (2018) 1145-1152.

[32] N. Cherkashin, N. Daghbouj, F. X. Darras, M. Fnaiech, A. Claverie, Cracks and blisters formed close to a silicon wafer surface by He-H co-implantation at low energy, J. Appl. Phys. 118 (2015) 245301.

[33] P. Moeck, S. Rouvimov, E.F. Rauch, M. Véron, H. Kirmse, I. Häusler, W. Neumann, D. Bultreys, Y. Maniette, S. Nicolopoulos, High spatial resolution semi-automatic crystallite orientation and phase mapping of nanocrystals in transmission electron microscopes, Cryst. Res. Technol. 46 (2011) 589–606.

[34] D. B. Williams, C. B. Carter, Transmission Electron Microscopy: A Textbook for Materials Science, second ed., Springer, Berlin, 2009.